Parameter Variation Overview:

In our recent LCROSS mission analysis, we wanted to match the Light curve and Blue/Red ratio curves from the Visible Spectrometer. We varied several spike and cone parameters in order to analyze each parameters' effect on the model data output. The parameters for the cone included: maximum cone grain velocity, average cone grain radius, and cone angle. The parameters for the spike included: maximum spike grain velocity, average spike grain radius, spike angle, and the fraction of the total mass in the spike plume. What follows are each of the parameter variation plots. For each plot, all but the chosen variable was held constant.

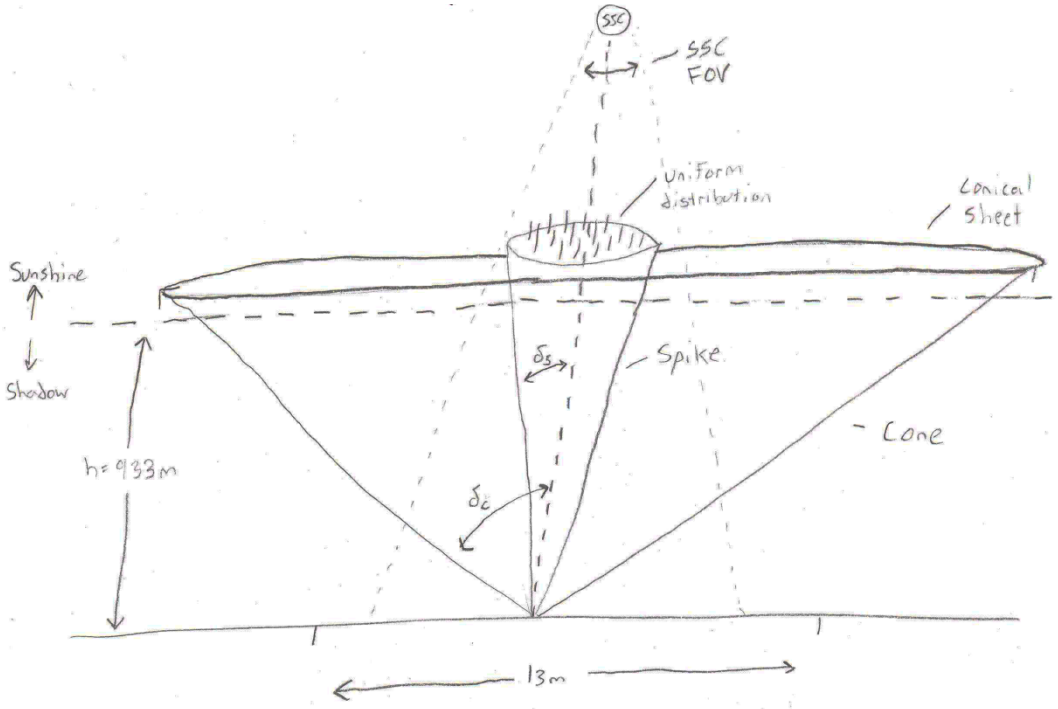

Assumptions and Approximations:

Impact Cratering model overview:

The impact crater model assumes a 13 m radius circular crater with an excavated mass, M_T =100,000 kg, of regolith in the form of a uniform density cylinder the width of the crater. The model makes the assumption that the density of an individual grain is 3300 kg/m^3 and that the regolith has a porosity of 70%. With these assumptions, it can be inferred that the cylinder has a depth of 19 cm. This cylinder is then divided into a cone and a spike section using the spike fraction (SpikeF, fraction of total mass in the spike). Each cylinder section contributes the mass to its respective plume components (see Figure 1). The cone and spike sections of the cylinder can be given different properties. These properties include: grain size distributions, ejection angles, and maximum velocities. For ejection angles, the spike grains can be given a distribution of angles. The cone grains are given a single angle value since the cone is

modeled as a single, conical sheet of particles. For maximum velocity, the model will ignore any particles that are faster than the given maximum.

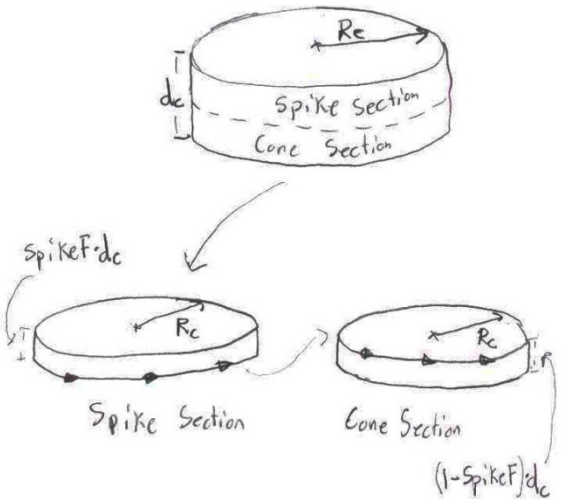

Figure 1 - Dirt cylinder divided into Spike and Cone sections

We use a model described in Cintala, Berthoud, and Horz (CBH) to correlate two parameters, grain velocity distribution and total amount of visible mass released, to the grain origin in the impact crater and the angle from the Moon's spherical surface normal. Grains are assigned to be either spike or cone grains according to the spike fraction and then assigned radii to fit the grain radius distribution corresponding to their respective plume component. They are also assumed to be distributed randomly in a uniform manner throughout the whole area of the 13 m crater. The distance between a grain's point of origin and the center of the crater (given by r in figure 2) dictates that grain's speed.

Equation 1 - velocity as a function of location in crater

$$v = C\left(\frac{r}{R_c}\right)^{-k}\sqrt{gR_c}$$

Here v is speed, r is the distance from the grain's initial location to the center of the crater, R_c is the ultimate radius of the impact crater, g is the gravitational constant at the lunar surface, and C=.49 & k=2 are constants determined from the CBH paper.

Through this process, a distribution of velocities is generated. Grains whose vertical velocities are too low to make it out of the crater and into sunlight are ignored–this lower limit to the velocity distribution, v_{-}, is given in Equation 2. This minimum velocity is also a function of the angle at which the grains are ejected, which differs between the spike and the cone. Very fast moving grains are also ignored (based on conversations with P. Schultz), with the upper limit, v_{+}, determined by an arbitrary cutoff which is also specific to each plume component.

Equation 2 - Velocity limits

$$v_{-} = \frac{\sqrt{\frac{2gR_{moon}h}{R_{moon}+h}}}{\cos(\theta)}$$

$$v_{+} = v_{lim}$$

Here, θ is the angle from the global surface normal, R_{moon} is the radius of the moon, and h is the height to sunlight (933m).

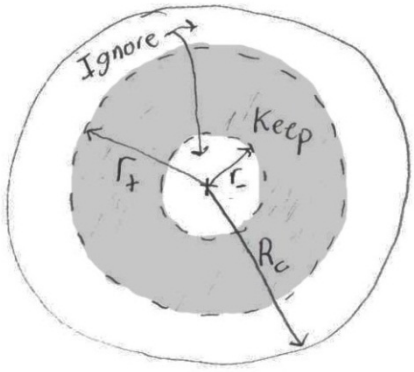

Figure 2 - Ring between radius limits where visible plume grains come from

By inverting Equation 1, we obtain an equation for the radial distance from the center where grains of a given velocity will be generated. The maximum and minimum velocity limits for both the cone and the spike are mapped to their respective radius limits. Thus, due to the two velocity constraints imposed on the cone component of the plume, we know that all of the grains used in the computation originated from the ring shaped part of the cone's mass disc, similarly for the spike.

Equation 3 - Radius limits as defined by velocity limits

$$r_{+} = R_c\left(\cos(\theta)C\sqrt{\frac{R_c(R_{moon}+h)}{2R_{moon}h}}\right)^{1/k}$$

$$r_{-} = R_c\left(\frac{C\sqrt{gR_c}}{v_{+}}\right)^{1/k}$$

Knowing that all of the regolith present in the sunlit plume originated inside the rings defined by the radius limits for each plume component, we can determine the mass which made it into sunlight and is therefore included in the model. As shown in Equation 4, the mass of each plume component is equal to the percent of total crater area covered by the ring of allowable velocities for that component multiplied by the mass of that component's mass disc shown in Figure 1.

Equation 4 - mass of each plume component (the sunlit part included in model)

$$m_{cone} = M_T(1 - SpikeF)\frac{{r_{+cone}}^2 - {r_{-cone}}^2}{{R_c}^2}$$

$$m_{spike} = M_T(SpikeF)\frac{{r_{+spike}}^2 - {r_{-spike}}^2}{{R_c}^2}$$

Plume Spectral model overview:

Spectral properties are calculated using a far-field approximation where the brightness of a particle is assumed to be independent of distance from particle to detector. Optical depths (scattering depths?) are then calculated with Equation 5, and assumed proportional to the brightness.

Equation 5 - Optical Depth

$$\tau = \sum_{j=1}^{N} \frac{A_j Q_j}{A_s}$$

τ is optical depth, A_j is the cross-sectional area (πr_{grain}^2) of the *j*th grain, Q_j is the ~~extinction coefficient~~ (Mie coefficient?) of the *j*th grain, N is the total number of grains and A_s is the area of the lunar surface in the field of view of the SSC. If we assume all the grains are the same size:

Equation 6 - Simplified Optical Depth

$A_j \approx A = \pi r_{grain}^2 \quad \forall j$, and $Q_j \approx Q \quad \forall j$, then $\tau \approx N\frac{AQ}{A_s} = n\pi r_{grain}^2 Q$

then we recover the common expression for optical depth, where r is the radius of the grains and n is the column density.

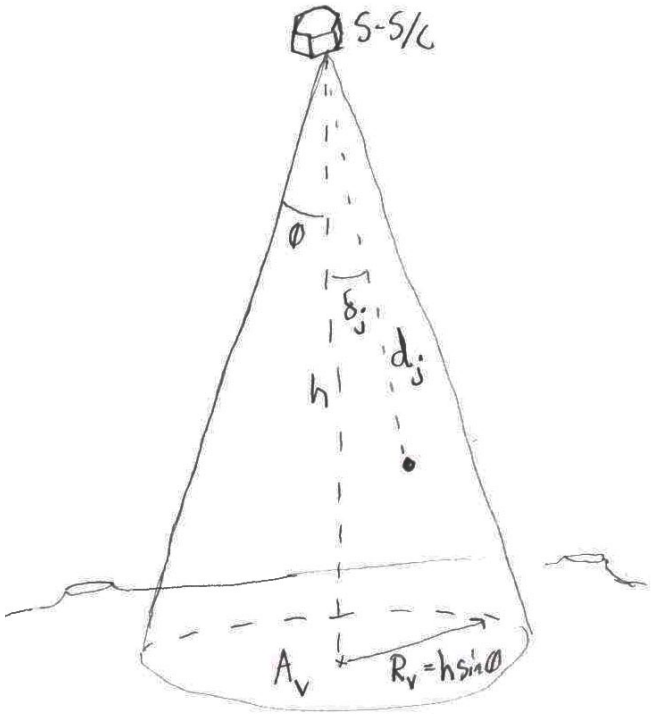

Figure 3 - Diagram of SSC viewing a grain

Values for Q come from the Cloud radiance excel sheet provided by Tony Colaprete. Q specific to wavelength was integrated from 260 nm to 650 nm for different grain radii to get the Q for the brightness, and then over 300 nm to 400 nm to get the Q values for the blue band, and from 550 nm to 650 nm to get the Q values for the red band (don't these values make it more like a violet to yellow&orange?). Blue/red ratios are computed by calculating τ using Q_{blue} and dividing by τ based on Q_{red}.

Nominal Case:

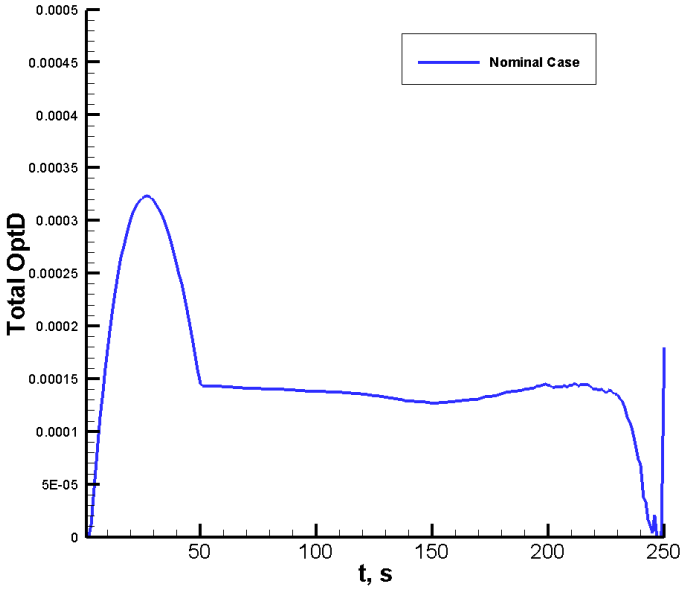

Figure 4 - Nominal Case

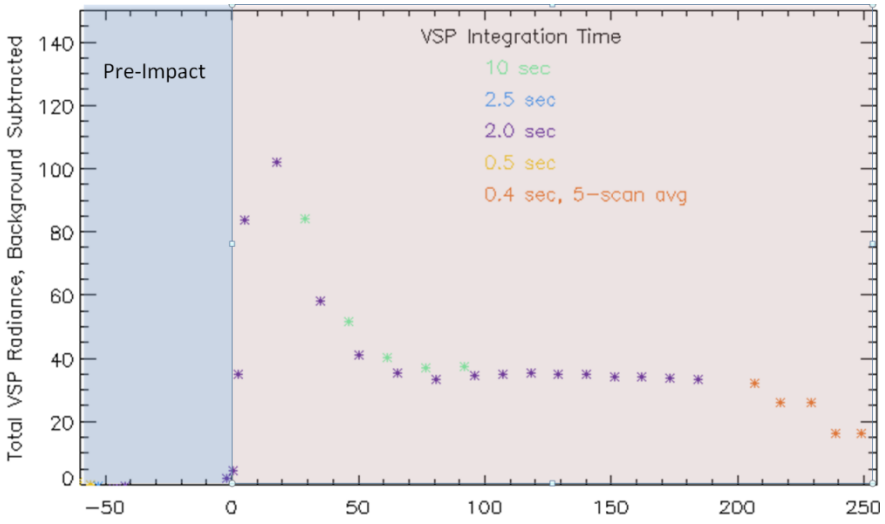

Figure 5 - Observed Radiance

Nominal Case Discussion:

Figure 1 displays the brightness for the nominal case based on the seven parameterized variables in the first table and the constant variables in the second table. The nominal case was constructed based off of the parameterization analysis performed using the seven main plume parameters. From this analysis, it was determined which features of the brightness plots were affected by each of the parameters. The values in the first table were chosen in order to get the shape seen in Figure 17. The two plots are similar in many of their features. Overall the basic shapes of the graphs are

largely similar with each having initial peaks followed by a leveling off until around 230 seconds. The first feature that should be noted is that the cone grains hardly contribute to the total brightness after around 50 seconds in both figures. This feature was matched by selecting the cone angle that leads to a leveling off in the model at around 50 seconds. Another feature that seems to match the observed brightness is the relative height of the initial peak when compared to the horizontal curve after 50 seconds. The heights of both of the peaks, modeled and observed, seem to be proportional in size.

There are a few differences between the observed plot and the nominal plot. The first one to notice is the point where the cone grains leave the field of view around 50 seconds. At this point in the nominal case, the radiance has a sudden, sharp leveling off. In the observed radiance plot, this transition around 50 seconds is more gradual. The second major difference is the brightness drop off towards the end of the plots. This can be explained in how the computer model handles particles that are stuck to the surface. The program checks if a particle has gone under the surface for each step. Instead of placing this particle at the surface, the program will keep the particle at the previous location—some point above the surface. This could contribute to the brightness curve not dropping off as the observations indicated. In the nominal case, the radiance seems to have a much more sudden drop off when compared to the observed radiance.

Main Plume Parameters (Nominal Case):

Parameter	Value
Spike Fraction	19.6%
Cone Grain Radius	1.2 microns
Cone Angle	55˚
Cone Grain Velocity Limit	800 m/s
Spike Grain Radius	0.8 microns
Spike Angle	10˚
Spike Grain Velocity Limit	1000 m/s

Other Plume/Moon Parameters:

Variable	Description	Value
meanalbedo	Mean Lunar Albedo	.12
prtden	Particle Density	3300 kg/m^3
T_ss	Sub-solar Temperature	370 K
T_ds	Dark Surface Temperature	120 K
finalR	Final Crater Radius	13 m
ex	CBH constant	2
const1	CBH constant	0.490
wmsfrc	Water (ice) Mass Fraction	6%
Qsunmx	Sunlight input	1370 W/m^2
dH_o_k	Binding energy of water on unannealed ice	4816 K
nu0inv	1/(Lattice vibrational frequency of ice?)	5.0e-13 1/s
CTtemp	Cold trap temperature	25 K

epslon	Particle emissivity	0.7
Srclat, srclon	Coordinates of Centaur impact	-84.675, -48.703
Ssclat, ssclon	Coordinates of SSC impact	-84.719, -49.61
crtrdp	Depth of Cabeus crater	883 m
h_min	Min. height to sunlight	863 m
h_max	Max height of crater	903 m

Simulation Parameters:

Parameter	**Description**	**Value**
ngrns	Number of Grains in simulation	80,000
nprts	Number of Particles per grain in simulation	6
nprtso	Code restart parameter (obsolete)	16,000
steps	Time Steps	250
delt_t	Time per step	1 s
nfnum	Exponent in relation: $\#H_2O\ mol\ \propto {r_{grain}}^{nfnum}$	3 (water is proportional to grain volume, ie mass)

Post-Impact Crater Spray Parameters:

Parameter	**Description**	**Value**
relsteps	Duration of spray release (in steps)	250
npartspr	Number of Particles in Spray in simulation	300
M_spr	Mass of water released by spray	23 kg
spraytemp	Temperature of Particle Spray	50 K

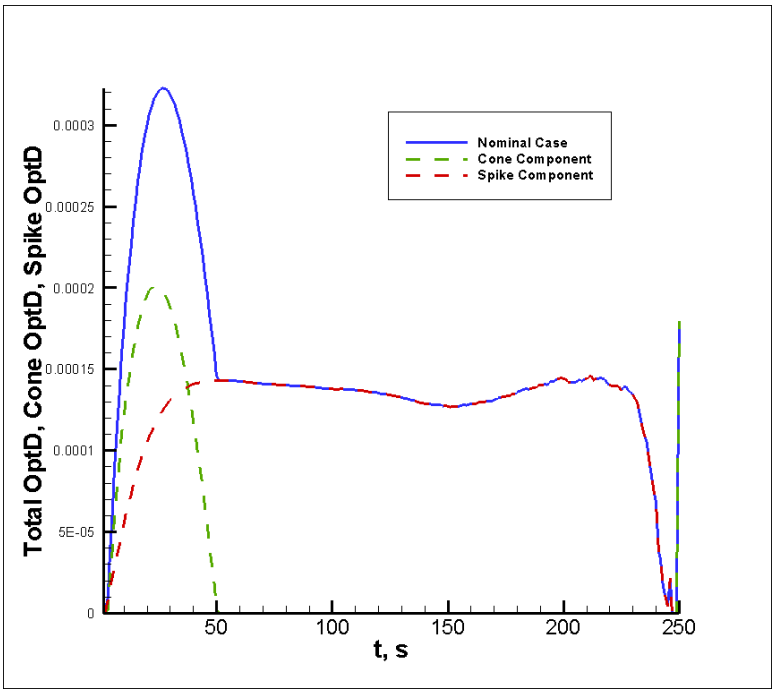

Figure 6 - Nominal Case with Cone and Spike contributions

Cone and Spike Distribution:

Figure 19 shows the nominal case from Figure 17 with dotted lines for the Cone and Spike contributions to the total radiance. The green dotted line is the cone component to the total radiance, and the red dotted line is the spike component to total radiance. The cone component's radiance plot follows physically what the cone component should do based off of the observations. The cone component is the largest contributor to the total plume mass; however, since the cone component is at a lower angle with respect to the surface the total time the grains will be in view is significantly shorter. This is confirmed by observing that the green cone line disappears at 50 seconds. Another observation that can be made is comparing the fraction of the total mass in each of the plume components with each of their contributions to the total radiance. In the nominal case, the fraction of mass in the spike was set at 19.6%. This value of 19.6% does not translate to the spike component contributing the same percentage to the total radiance. The first 50 seconds shows that the spike contributes at least 50% to the total radiance after about 10 seconds. This makes sense due to the spike component having a much larger angle with respect to the surface and; therefore, a higher maximum height. This would make one believe that the spike component would be in view longer and contribute more per grain to the total radiance.

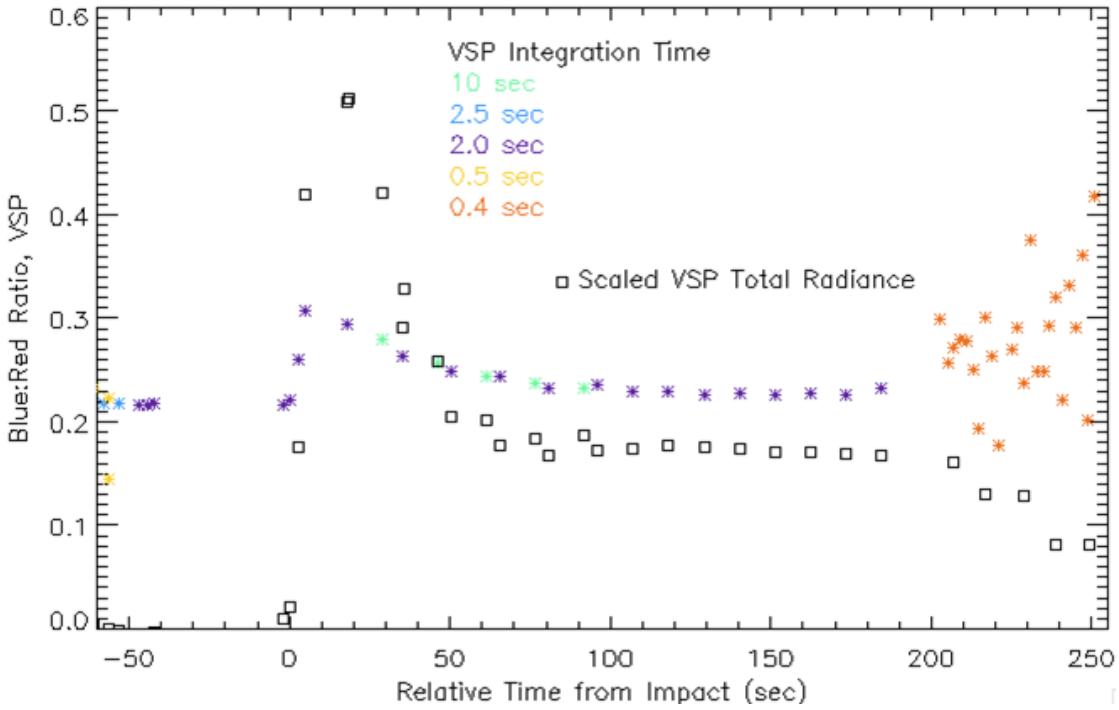

Figure 7 – Observed Blue/Red Ratio

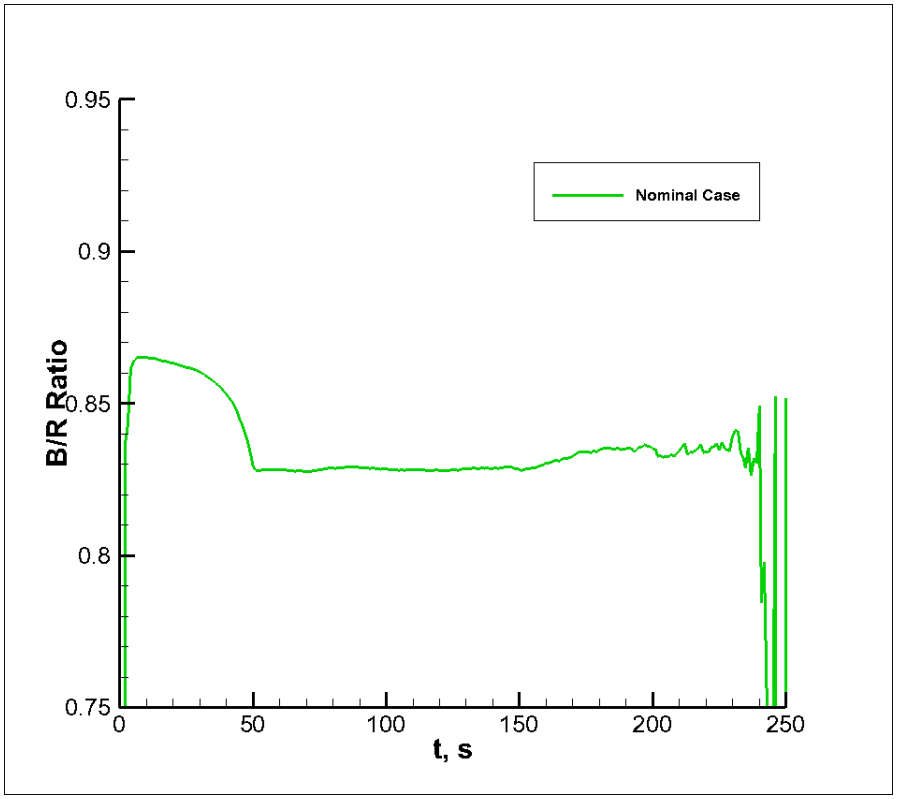

Figure 8 – Nominal case Blue/Red ratio

B/R ratio Discussion:

Figure 8 shows the B/R ratio for the nominal case described in the tables above. Comparing with the observed ratio in Figure 7, we see the same trend consisting of a rise in the blue/red ratio, we see the same rise in blueness that levels off and remains constant afterwards. The sharp rise occurs within the first five seconds, and then continues decreases slightly. At 45 seconds, the curve transitions to a sharp drop and by 50 seconds it flatlines. Differences from the observed data include the values for the b/r ratios themselves being much greater than the observed data, hovering in the ~.84 range rather than the ~.25 range. The model also predicts a sharp corner in the b/r plot (as it did for the brightness plot in Figure 4), caused by the cone grains exiting practically all at once. In comparison, Figure 7 shows a more gentle transition from the drop in b/r ratio to the flatline (as it does for the brightness), suggesting that the cone component of the plume did not leave the field of view all at once. This effect can be simulated in the model in the same manner as the spike, that is, by assigning a distribution to the cone angles rather than a single value.

Parameter Variations:

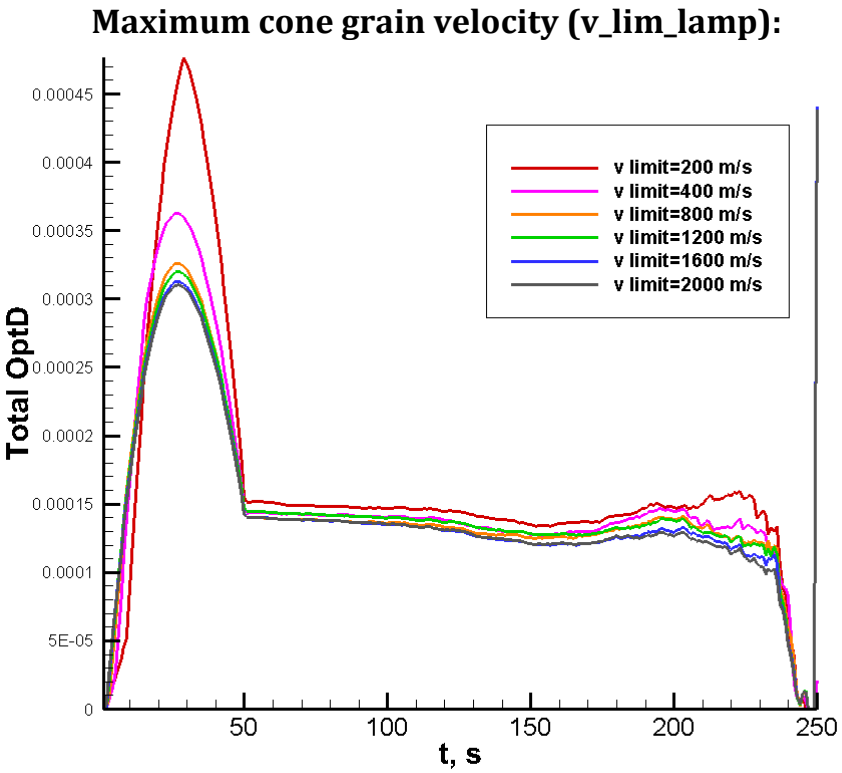

Figure 9 - Radiance vs. Time plot with cone velocity limit variation.

We first examine the effect of varying the cone velocity limit, $v_{\mathrm{lim,cone}}$. The velocity limit for the cone grains seems to have a minimal effect on the brightness vs. time (Fig. 4). Not much variance is seen in the first 50 seconds when the cone is in view. Side note: the reason for the upward trend after 50 s is that a very small spike angle was used for these runs.

The variation after 50 seconds when only the spike is in view is likely an effect of the impact cratering model we used to determine velocity distributions. As the velocity limit is lowered, the code will cut off more grains in the upper range of the speed spectrum. The model interprets a lower maximum velocity for the grains as a sign that less impact mass was able to make it out of the crater and into the sunlight, therefore the plume and the spike each had slightly less mass, hence the lower brightness.

Cone grain radius:

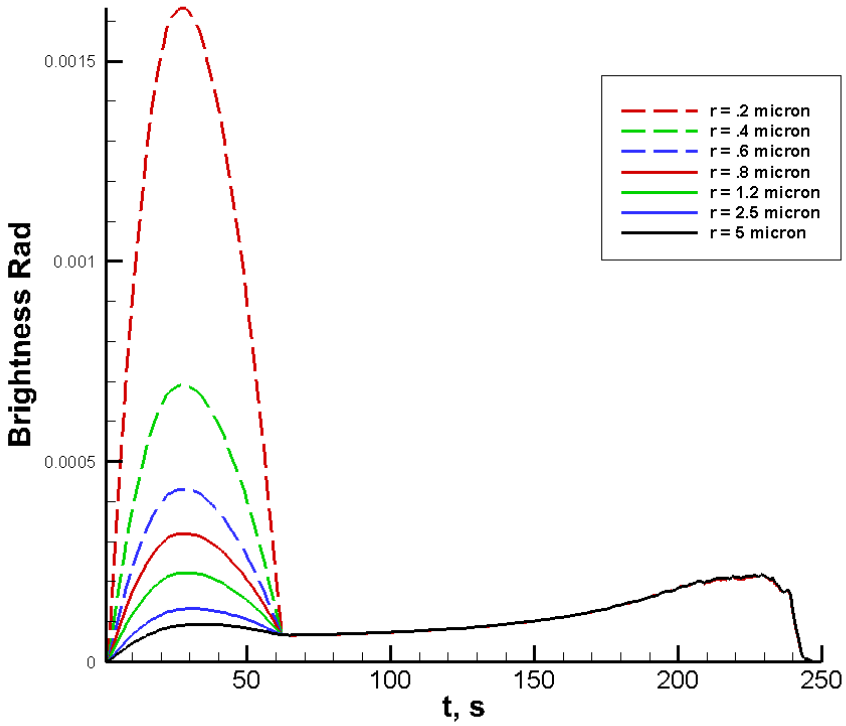

Figure 10 - Radiance vs. Time plot with cone radius variation.

Next, we consider the effect of varying cone particle radius. Figure 10 shows the variation in the resulting brightness when the average radius (microns) of the cone grains is varied from .2µm to 5µm while holding the total mass of the cone plume constant. As can be seen, as one increases the assumed average radius of cone grains, the peak brightness of the first peak decreases. This happens because the surface area of each grain varies proportional to the grain radius squared, but the total number of grains in that plume component varies as $\frac{1}{r^3}$, leading to a dramatic rise in brightness proportional to $\frac{1}{r}$ as assumed grain size is decreased. After ~ 60 seconds, the cone grains leave the field of view of the SSC, and variations in the average grain radius of the cone cease to affect the solution.

Cone angle:

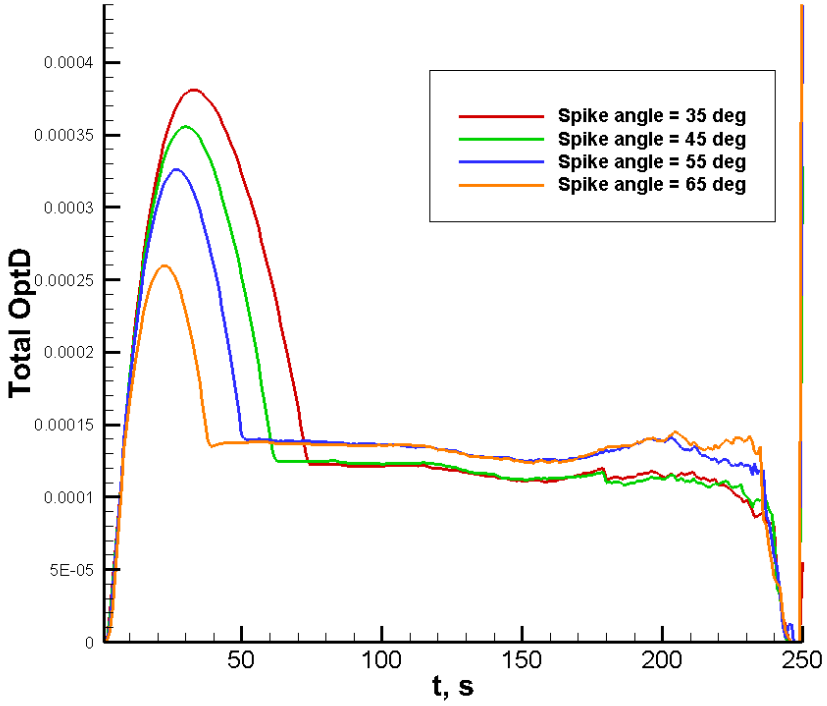

Figure 11 - Radiance vs. Time plot with cone angle, d, variation.

Figure 11 shows how changes in the cone angle will affect the observed brightness. The most important feature of this figure is that it shows that the cone angle determines the time when the cone plume leaves the field of view completely, seen shortly after the kink in the curve at 30 to 80 seconds. This time seems to be clearly determinable from the observations and could thus constrain the cone angle.

Another feature to note is the large difference in peak brightness of the maximum attributed to the cone. The cone angle in this case is measured with respect to the surface normal of the moon (note: as in, normal to a spherical moon, an axis that would pass through the center of the moon, not to be confused with the actual surface normal of the impact site). The figure shows that smaller cone angles, for more spike-like cones, lead to larger peak brightness values. This effect upon the brightness is likely another effect of the impact cratering model. Low cone angles signify that vertical velocity component of the cone grains is greater than the outward radial component, and therefore a larger fraction of the cone mass is capable of making it out of the crater and into sunlight, yielding a higher brightness for low cone angles [see Figure 2]. For this same reason, low values of d imply that the radial component of the velocity was low, so it would take longer for lower angle cone particles to move far enough away radially (away from the axis) to be out of sight of the SSC. Therefore, lower cone angles mean that the cone would be in view longer.

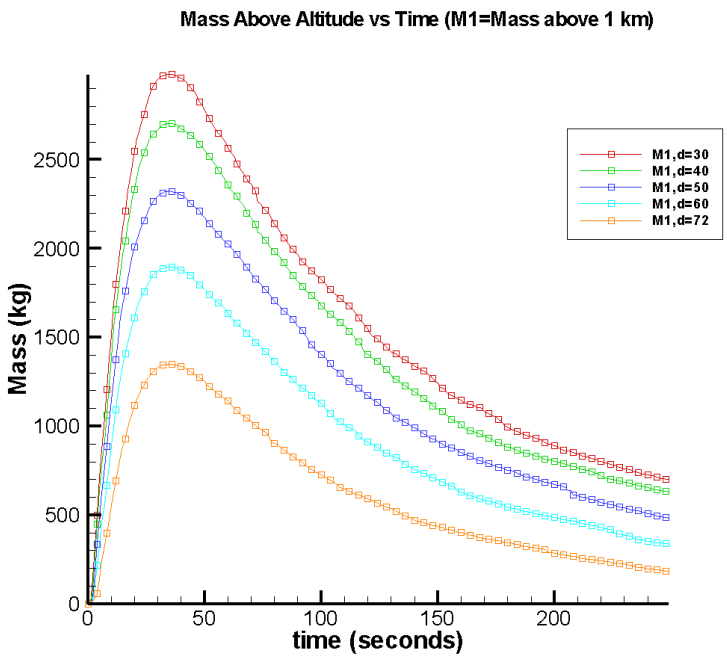

Figure 12 - Mass above 1km Altitude vs. Time with cone angle variation

Figure 12 shows the mass above one kilometer for a range of cone angle values. The figure supports the above point that with lower angles one would find a greater fraction of total velocity in the vertical component and therefore more mass reaches sunlight. The plot clearly shows that the mass above one kilometer increases as the cone angle is decreased.

Fraction of mass in spike component:

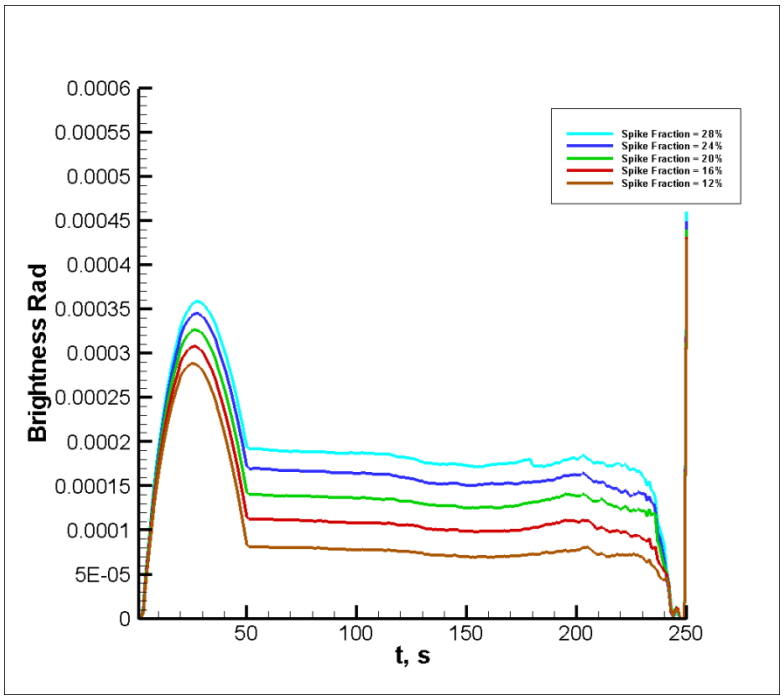

Figure 13 - Radiance vs. Time plot with spike mass fraction variation.

Figure 8 displays the brightness variation when the fraction of the total mass that is in the spike, SpikeF, is changed. Increasing SpikeF increases the brightness throughout the plot. The increase is more pronounced in the portion that is after 50 seconds since the spike is the only component in view after the initial peak. An interesting result occurred, however, in the initial peak portion of the plot. The spike grains had an effect on the cone brightness peak; however, the larger increase in brightness occurs towards the latter part of the peak. A possible explanation for this is up until the top part of the initial cone peak, the brightness observed by the SSC has little to do with which plume component the grains are in. At the top of the peak, grains from the cone portion began to leave the field of view and this is why we see a drop off in brightness at around 50 seconds. With more mass in the spike, less of a decrease in brightness is observed.

Spike angle:

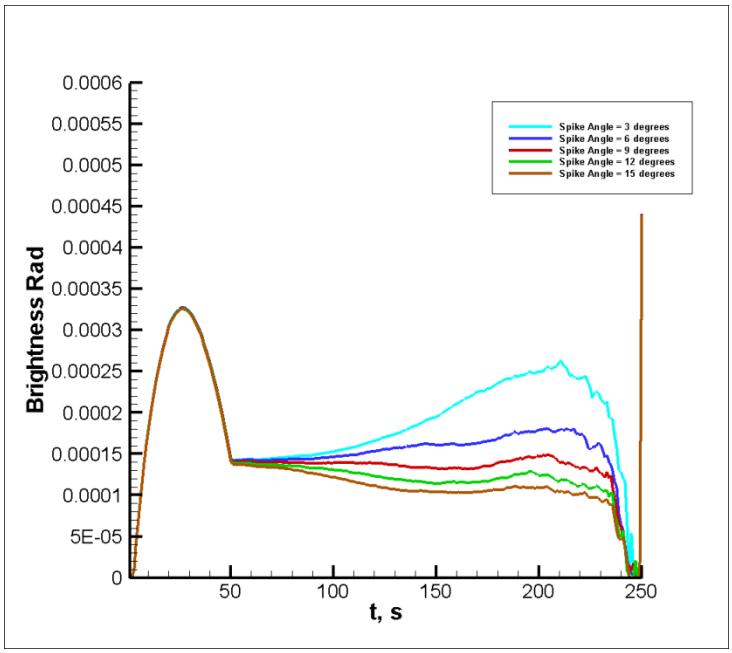

Figure 14 - Radiance vs. Time plot with spike angle variation.

Figure 9 shows the effect of variation of the spike angle from 3 degrees to 15 degrees. Seen in the plot, variations in the spike angle change the slope of the portion of the plot after 50 seconds. This is likely due to there being more mass in view longer for lower spike angles, and therefore more brightness. With very low spike angles, the spike is traveling almost entirely up and barely spreading, meaning it spends most of its time in the field of view. In fact, for very narrow (around 3 degrees) spikes nearly all of the spike material largely remains in the FOV until around 200 seconds when the SSC begins to enter the top of the spike portion of the plume. When the spike angle is higher, the spike spreads more and more mass leaves the field of view more rapidly. The angle-velocity correlations in the impact cratering model could possibly have affected the brightness as well, lowering the velocity for lower spike angles.

Spike angle distribution:

Unlike cone grains which can only travel in a sheet at the cone angle, spike particles are allowed to have an angle anywhere between 0 and the spike angle. The distribution of grain angles has a very important effect on the brightness at later times. Three distributions of spike angles were tested, varying the max spike angle for each: an inverse square root distribution, a sinusoidal distribution (leads to uniform distribution over a spherical cap), and a dirac delta distribution at the max spike angle (every grain travels in a sheet at the max spike angle). Figure 15 shows the probability distribution functions of these three distributions graphed, for a maximum spike angle of 3°. For reference, all runs outside of this section used an inverse square root distribution.

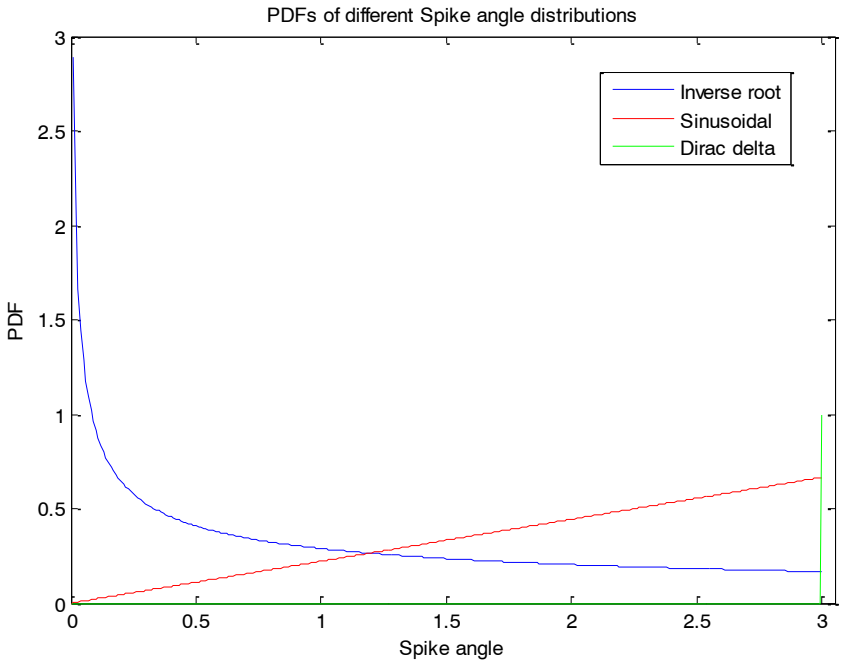

Figure 15 - Graph of the 3 spike angle distributions

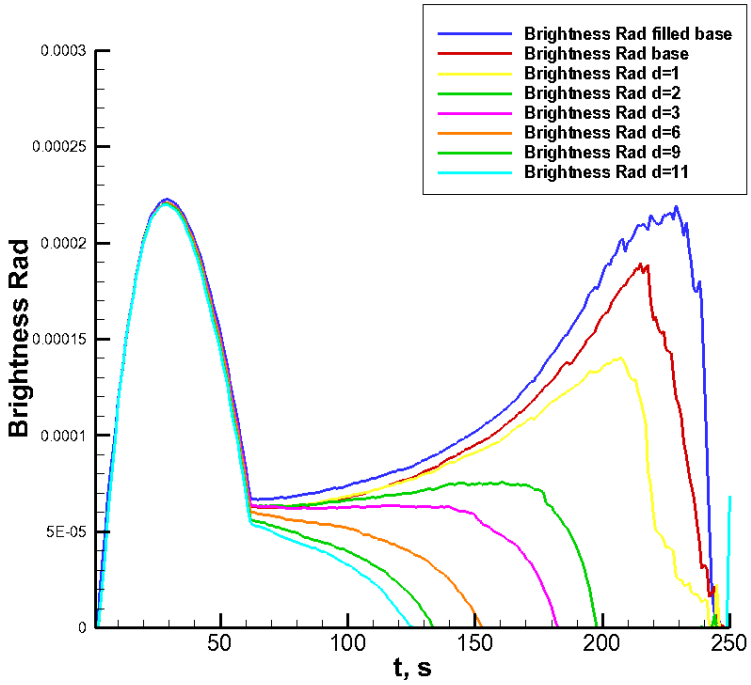

Figure 16 - Radiance vs. Time plot for varying spike angle with dirac delta distribution

Figure 16 shows brightness dropping to zero before the SSC impacted the moon. The time at which brightness goes to zero and the brightness after 70 s both increase with decreasing spike angle. This trend is similar to the trend seen in Figure 14 but much more pronounced. Figure 17 shows brightness decaying slowly to zero, but following the same general trend as the other three distributions of

decreasing spike angle leading to an increase and a peak in brightness at later times. As the section on spike angle variation detailed, grains at larger angles leave the field of view of the SSC earlier whereas grains at very small angles take longer to leave the field of view.

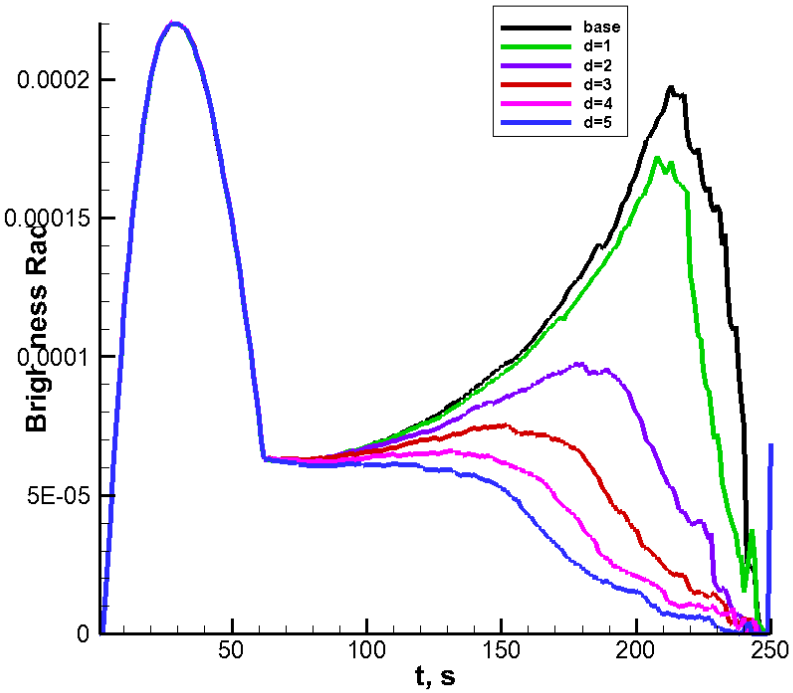

Figure 17 – Radiance vs. Time plot for varying spike angle with sinusoidal distribution

It is noted that a delta distribution of spike angles (Figure 15), which leads to the sharpest and earliest drop in brightness of the 3 distributions for a given spike angle, also happens to be the distribution which weighs the higher spike angles the heaviest. It is also important to note from Figure 16 that there does not exist a maximum spike angle which will exhibit nearly constant brightness until 200 s as shown in the LCROSS data. Therefore, the spike grains could not have all traveled at the same angle (i.e., the spike was not hollow, it had to have been 'filled' in some way by a distribution of different spike angles). The distribution which weighs the smaller angles most heavily (Inverse square root) also is the one which shows the least drop in brightness as spike angle increases, and has the highest brightness of the 3 for a given angle. The sinusoidal distribution, the most balanced of the 3 distributions (actually, gives a perfectly uniform spherical distribution of grains), shows a combination of the traits of the other two.

Of all the cases run, using an inverse square root distribution with a max spike angle of 9° gives the best fit, in that it shows a nearly constant brightness all the way to 200 s. However, the sinusoidal distribution has the slow drop off in brightness characteristic from 200 s to 250 s as shown in the data, a feature which is not present in the inverse square root distribution.

Maximum spike grain velocity:

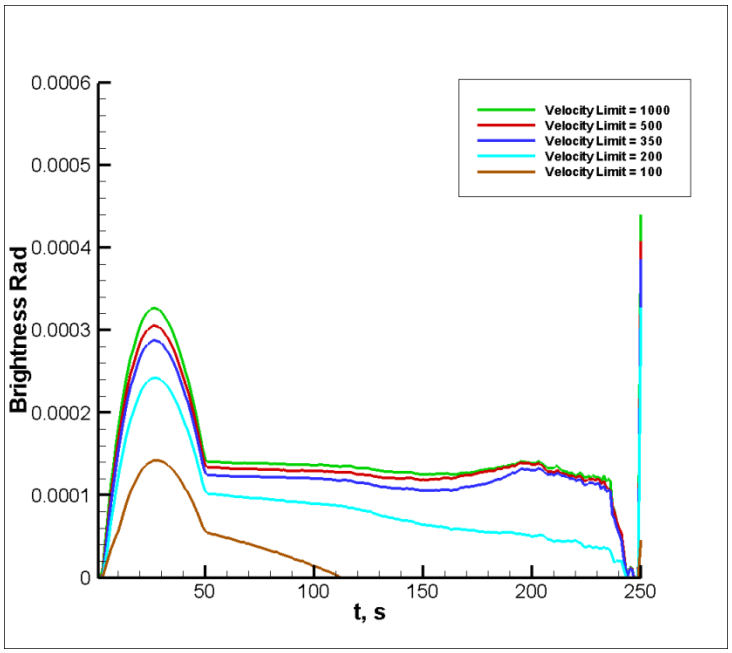

Figure 18 - Radiance vs. Time plot with spike velocity limit variation.

Figure 13 shows how the brightness changes as the maximum limit on spike grain velocity is varied. As seen, the drop-off occurs sooner with a low velocity limit. There are two processes at work here. First, lowering the velocity limit for spike grains makes all the spike grains slower. Slow grains do not stay aloft long and soon fall back down to the lunar surface. We don't see this early disappearance of grains for higher velocity limits; brightness only drops off in the cases below a cutoff speed of 350 m/s as the SSC flies through the plume. The second process is due to the impact cratering model, where a lower velocity limit leads to less mass in the plume, as explained in the cone velocity limit section. The peak brightness during the time the cone is visible drops as the velocity limit is lowered, hinting that less mass is visible at the time and providing support for this second process being as work, since more slowly rising particles rise into view more gradually.

Mass above Altitude for Spike Velocity Limit:

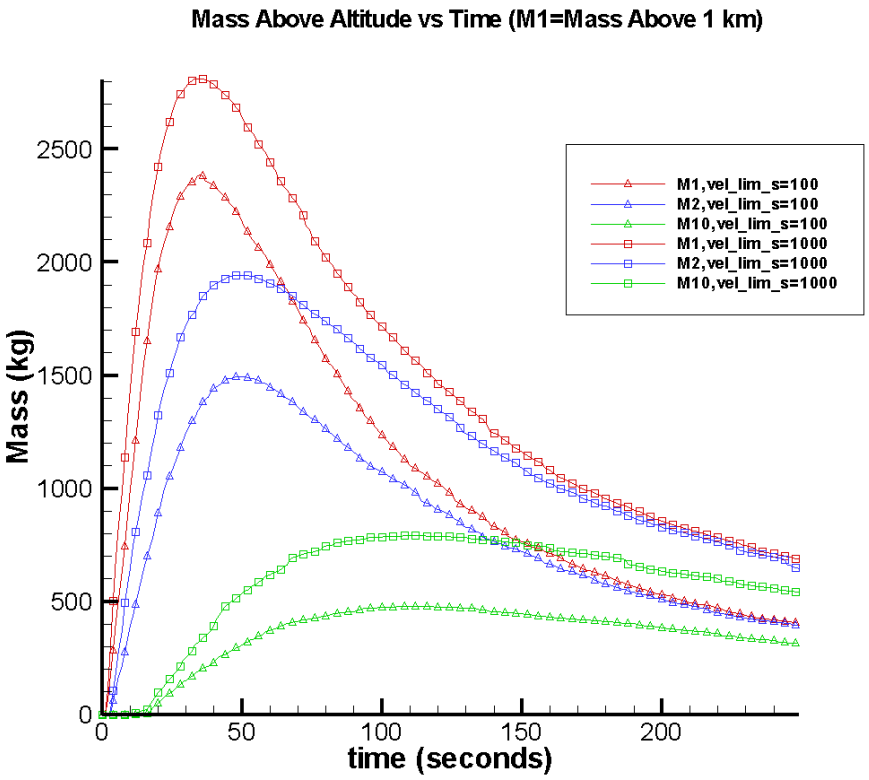

Figure 19 – Mass above Altitude vs. Time Plot with spike velocity limit variation

Spike Velocity Limit (m/s)	Total Mass in Sunlight (kg)
1000	3314
500	3270
350	3232
200	3138
100	2917

Figure 20 - Total mass in sunlight for each spike velocity limit

Figures 14 and 15 are included in order to explain the curves in figure 13—the radiance plot where spike velocity limit was varied. Figure 14 has three pairs of curves for the upper and lower spike velocity limit values that were chosen. As you can see, with a lower velocity limit the less mass you have that gets above certain altitudes. This can explain the change in radiance seen in figure 13 where the radiance went down as the spike velocity limit was lowered. Figure 14 simply illustrates this point further—it shows the actual numerical values of total mass in sunlight from the simulation. Again, as the spike velocity limit is lowered, the total mass above a certain altitude is lower.

Spike grain radius:

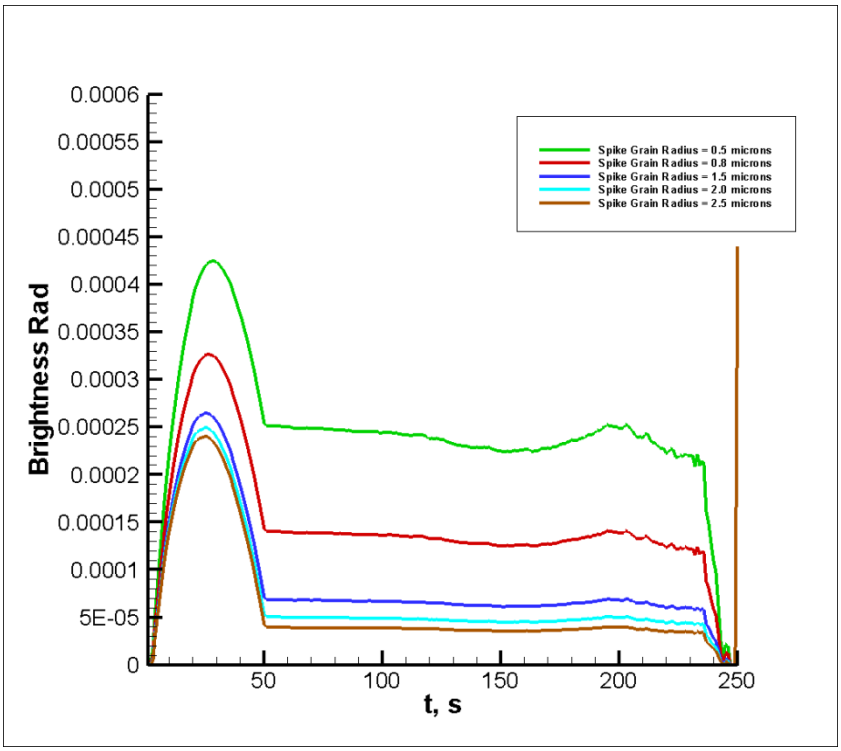

Figure 21 – Radiance vs. Time with spike radius varied

Figure 16 shows the variation of the brightness as the average spike grain radius is changed. The spike grain radius seems to act as a rough scaling factor for the brightness plot, for the same reasons that changing the average cone grain size affects brightness. The initial peak due to the cone contribution does not seem to change its absolute height compared to the flat portion past 70 seconds.